ACS Catalysis

RESEARCH ARTICLE

pubs.acs.org/acscatalysis

Density Functional Theory Study of Alkane-Alkoxide Hydride Transfer in Zeolites

Gregory M. Mullen and Michael J. Janik*

Department of Chemical Engineering, The Pennsylvania State University, 104 Fenske Laboratory, University Park, Pennsylvania 16802, United States

Supporting Information

ABSTRACT: A solid acid catalyst for the production of alkylation gasoline is sought to replace hazardous strong liquid acids currently used. An optimal catalyst for this application must be able to readily promote hydride transfer between alkyl groups to facilitate sustained activity. Herein, periodic density functional theory (DFT) is used to evaluate the energetics of hydride transfer over acidic mordenite for various combinations of hydride donor and acceptor substitution. Dispersion corrections to DFT (DFT-D) are implemented to better represent non-bonding interactions between the reactive species and the zeolite framework. DFT predicts an increasingly endothermic energy to incorporate the alkane into the zeolite pore as the hydride-donor molecule size increases. However, the inclusion of dispersion energy corrections shifts these energies to exothermic values, and a non-monotonic trend indicates a size dependent competition between attractive dispersion interactions and steric repulsion. The transition states for hydride transfer are mainly carbenium ions. Shared hydride carbonium ions represent metastable intermediates in most cases, with the notable exception of transfer between isobutane and the *t*-butyl alkoxide, for which the shared hydride species is more stable than its precursor and represents a global minimum along the hydride transfer reaction coordinate. Generation of a shared hydride intermediate from species localized within the pore shows an inverse monotonic trend between formation energy and both donor and acceptor substitution. Activation energies for the elementary step of shared hydride complex formation also show an inverse monotonic trend with respect to donor and acceptor substitution. Dispersion energy considerations decrease the overall barrier to hydride transfer in most cases.

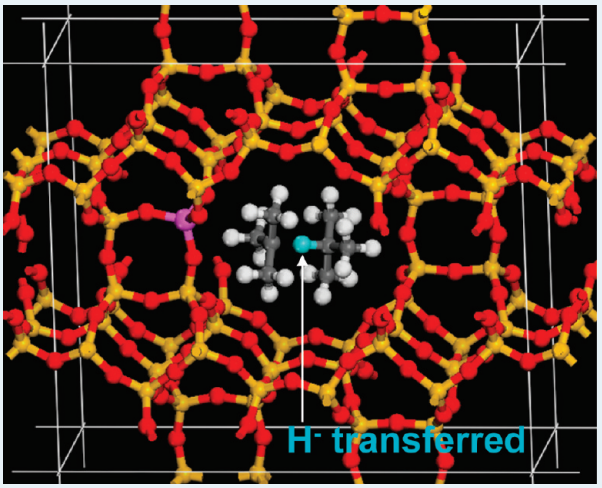

KEYWORDS: zeolites, mordenite, hydride transfer, alkylation, DFT+D

INTRODUCTION

Significant efforts have been directed toward the discovery of a suitable solid acid catalyst to replace strong liquid acids currently used to produce alkylation gasoline. Although, in principle, many solid acids are capable of catalyzing the reactions involved in these processes, a practical option for large-scale implementation has yet to be discovered. Zeolites are among the most promising replacement catalysts studied, displaying high initial activity and selectivity toward C8 products, in addition to thermal and hydrothermal stability.[1] However, like many other solid acid catalysts, they suffer from rapid catalyst deactivation, generally accepted to result from an insufficient ability to promote intermolecular hydride transfer.[2−6] Catalyst deactivation remains the foremost challenge in the search for a viable catalyst.[3] Thereby, a thorough understanding of the effects of local catalyst structure on the energetics governing the hydride transfer mechanism is necessary for the assessment of a potential catalyst for large-scale implementation. Previous studies have identified potential intermediates and transition states for hydride transfer reactions occurring both in gas phase and over solid acid catalysts.[7−11] Herein, we utilize periodic density functional theory (DFT) to evaluate the energetics of hydride transfer over mordenite for various combinations of hydride donor and acceptor substitution.

Zeolites exhibit high initial activity for alkylation and selectivity toward C8 alkane products. However, in zeolite catalyzed alkylation processes, both activity and selectivity decrease with time on stream.[2−4,12] This behavior is typically coupled with an increase in the production of heavier alkanes in the product stream. At long enough reaction times, alkylation products cease to be generated. Large quantities of heavy hydrocarbons typically collect in the deactivated zeolite catalysts. The loss of catalytic activity has been proposed to result from a decreased ability to promote the transfer of a hydride (H^-) species from an alkane to the adsorbed, growing alkoxide chain.[2−6]

Received: October 20, 2010
Revised: December 15, 2010
Published: January 18, 2011

Zeolite catalyzed isobutane-butene alkylations are thought to proceed by the same general mechanism as liquid acid catalyzed alkylations.[1] A simplified view of the mechanism involves a propagated chain reaction, initiated by butene protonation and simultaneous chemisorption to yield an s-butyl species,[1] commonly referred to as an alkoxide, at the zeolite's acid site. This species abstracts hydrogen from isobutane in the process of hydride transfer, desorbing as butane and generating a *t*-butyl alkoxide in its place at the active site, which undergoes alkylation with butene to yield a C8 alkoxide. This species may isomerize, then desorbs via hydride transfer from an isobutane molecule, generating a C8 alkane and propagating the mechanism by restoring the *t*-butyl alkoxide. Competition between hydride transfer and alkylation is necessary to promote continued catalytic production of C8 products. The hydride transfer reaction must proceed rapidly enough to transform alkoxides into alkanes before multiple alkylations can occur. Otherwise, heavy hydrocarbons form within the pore, which results in deactivation of the catalyst.

The size of the zeolite pore has a significant influence on the alkylation chemistry that occurs within it. Corma et al. showed that alkylate yield, defined as mass C5+ generated per mass 2-butene charged, increases as the zeolite pore size increases for isobutane/2-butene alkylation.[13] Mordenite, a zeolite with a unidirectional pore formed by a 12-membered ring, exhibits a high alkylate yield.[13] Mordenite is also highly selective to C8 products for isobutane/2-butene alkylation processes, predominantly generating trimethylpentanes in its initial stages of activity.[12,13] As with other solid acid catalysts, mordenite does suffer from rapid deactivation in alkylation processes,[12,13] but its high initial activity and selectivity toward trimethylpentanes makes it among the most promising of solid acid catalysts for refinery alkylation processes.

Computational chemistry calculations based on first principles can provide insight into the dynamics of complex chemical systems. Density functional theory (DFT) studies have shown that the hydride transfer mechanism over many solid acid catalysts proceeds through the formation of metastable carbonium-ion intermediates in which hydrogen is shared between two alkyl species.[10,11] These intermediates are generally thought to form through carbenium ion transition states, analogous to structures seen in superacid media.[5,6] Cluster model DFT studies have indicated that hydride transfer over zeolites likely proceeds through this mechanism.[9,10] In the cluster approach, the active site is modeled by a small group of tetrahedral silicon−oxygen and aluminum−oxygen molecules. Though such models represent interactions between the active site and the hydrocarbon complexes generated in the reaction, they do not account for interactions between the hydrogen-sharing complex and zeolite pore. The spatial configuration of the zeolite pore limits the size of transition states and reaction intermediates capable of forming within its volume. Additionally, pore confinement may lead to site recognition of species involved in zeolite-catalyzed reactions, directing reaction selectivity.[1] Consequently, the pore configuration of the zeolite could prove significant in controlling the energetics of hydride transfer reactions. Advances in computational power have made viable the study of zeolites utilizing a period approach, which models the entire pore rather than simply the active site.

DFT is the most commonly used method for modeling systems of relevance for heterogeneous catalysis, offering insightful energetic and structural representations without requiring excessive computing power. However, DFT is subject to inherent deficiencies when describing van der Waals interactions.[14,15] Such interactions could affect the stability of intermediates and transition states involved in hydride transfer. The crystalline pore structure of zeolites makes them more subject to significant dispersion interaction effects than nonporous solid acid catalysts. Wave function-based methods of incorporating these forces are computationally intense and are beyond the scope of current computational capabilities for large zeolite models. However, dispersion energies can be accurately estimated with simple fitting functions based on empirical data. The addition of empirical dispersion interaction corrections to DFT, denoted DFT-D (density functional theory-dispersion), models bimolecular dispersion interactions with atom pair dispersion coefficients (C_6 coefficients), providing a semiempirical means to account for dispersion energies.[16,17] This method requires far less computational power than wave function-based methods, making it a viable means of including van der Waals energy contributions within an electronic structure calculation.

In the current study, we examine hydride transfer energetics using a periodic DFT model of mordenite, investigating donor and acceptor combinations of various sizes and degrees of carbon substitution. We consider the presence of the extended pore framework and the effects of hydrocarbon substitution on mordenite's ability to promote this reaction step and employ a DFT-D computational package to examine the effects of dispersion interactions.

COMPUTATIONAL METHODS

Electronic Structure Methods. Calculations were performed with the Vienna ab initio simulation package (VASP), an ab initio total energy and molecular dynamics program developed at the Institute for Material Physics at the University of Vienna.[18−20] Ultrasoft pseudopotentials (US-PP) were used to describe electron-ion interactions,[21] and the Perdew−Wang (PW91) form of the generalized gradient approximation (GGA) was used to include exchange and correlation energies.[22] An energy cutoff of 450 eV was used for the plane-wave basis set to represent valence electrons. Structural optimizations were performed by minimizing the forces on all atoms to below 0.05 eV $Å^{-1}$. The basis set, structural optimization criteria, and k-point sampling (discussed below for each model) were confirmed to converge the total energy to within 0.03 eV.

Transition states were identified using the climbing image nudged elastic band (NEB) method.[23−25] This method determines the minimum energy path between a known reactant and product pair by optimizing a chain of intermediate images between the two states, which are constrained such that each image maintains nuclear spacing with its neighboring images. The transition state, located at the saddle point of this path, was taken as the image of highest energy with a low absolute tangential force and atom forces equivalent to those of a structural optimization.

Model Construction. The mordenite unit cell (Figure 1) was constructed with 145 atoms ($Si_{47}AlO_{96}H$); 48 tetrahedral sites (T-sites) consist of a silicon or aluminum atom surrounded by four oxygen atoms with a hydrogen atom to balance the Bronsted acid generated at the aluminum T-site. Structural optimization with VASP yielded lattice vectors a = 18.094 Å, b = 20.516 Å, and c = 7.524 Å. These vectors are in good agreement with experimentally determined mordenite unit cell lattice vectors.[26−28] The main channel of the optimized structure consists of an elliptical, 12-membered ring, projected along the *c*-axis. All reactions were considered to occur within this pore. Including reactants, the largest systems consisted of 171 atoms ($Si_{47}AlO_{96}C_8H_{19}$). Fourteen combinations exist for placement of aluminum at four different T sites and placement of a proton at a distinct oxygen position in mordenite (Figure 1). Aluminum was placed in the T4 position and the

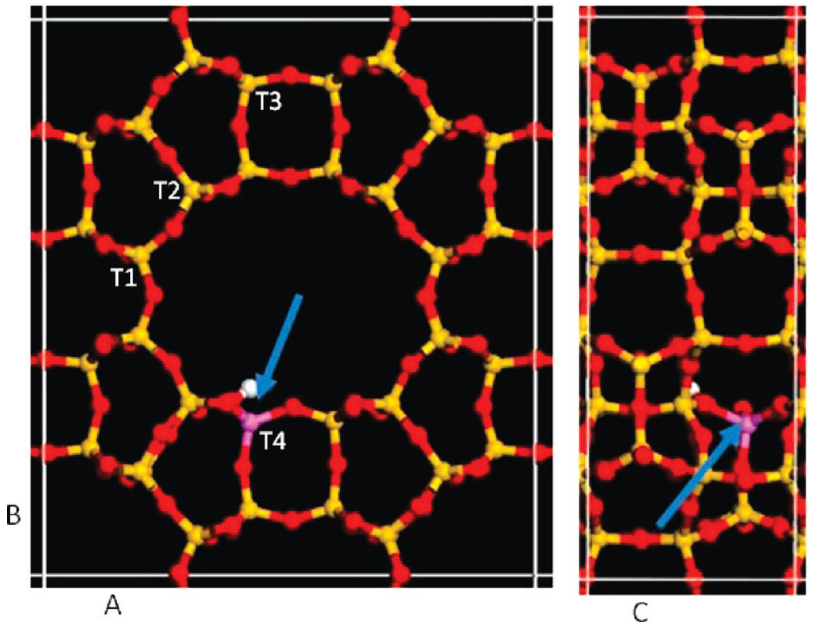

Figure 1. Mordenite unit cell. Al is located at the T4 position, marked with an arrow. The VASP optimized dimensions of the unit cell are a = 18.094 Å, b = 20.516 Å, and c = 7.524 Å.

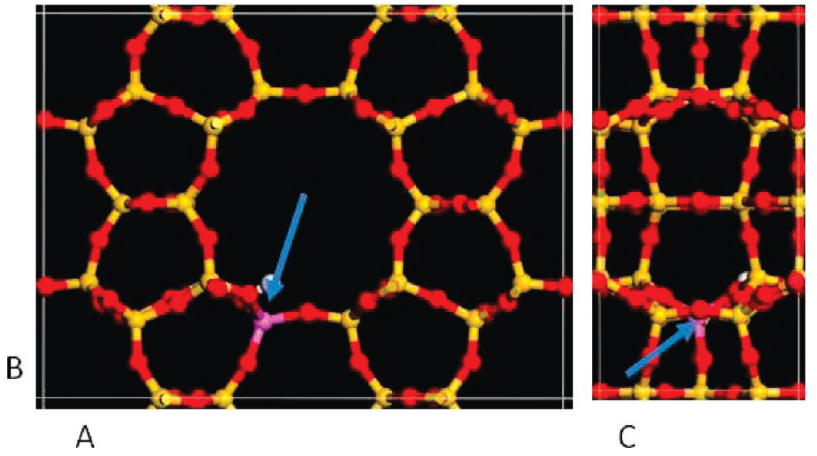

Figure 2. Ferrierite unit cell. The VASP optimized dimensions of the unit cell are a = 19.156 Å, b = 14.127 Å, c = 7.489 Å.

proton/alkoxide at the O2 site, corresponding to the lowest energy structure for mordenite with an Si/Al ratio of 47 as suggested by Brandle and Sauer[29] (numbering by Alberti[30]). The aluminum T-site is indicated with an arrow in Figure 1. The Brillouin zone was sampled using a (1 × 1 × 2) Monkhorst−Pack (MP) grid[31] with the third vector extended along the zeolite c-axis (Figure 1).

We performed a subset of calculations over acidic ferrierite. The ferrierite unit cell was constructed with 109 atoms ($Si_{35}AlO_{72}H$) (36 T-sites with a hydrogen atom to balance the Bronsted acid site, Figure 2). Structural optimization with VASP yielded lattice vectors a = 19.156 Å, b = 14.127 Å, c = 7.489 Å, which are also in good agreement with experimentally determined ferrierite unit cell lattice vectors.[32] The main channel of the optimized structure consists of an elliptical, 10-membered ring. The unit cell was optimized with Al and proton placed at the same sites as chosen by Tuma and Sauer.[33] The Brillouin zone was sampled using a (1 × 1 × 2) Monkhorst−Pack (MP) grid[31] with the third vector extended along the zeolite c-axis (Figure 2).

Alkoxide species, alkyl groups covalently bonded to oxygen in the zeolite framework (Figure 3a), form via protonation of alkenes at the unit cell's active site[34−37] for ethyl, propyl, and t-butyl alkoxides and via activation of methane for the methyl alkoxide.[38] These alkoxides represent stable states to which hydride transfer may occur. Alkoxide formation processes were not evaluated herein. Starting with the optimized alkoxide structures, alkane species were introduced nearby within the zeolite pore (Figure 3b). The hydride transfer reaction has been shown computationally to occur through the formation of metastable H-shared intermediates over zeolites[9,10] and other solid acid catalysts.[11] Shared hydride intermediates, optimized in the gas phase, were introduced into the zeolite pores near the active site (Figure 4), and the structure was optimized (Figure 3d). The H-shared structure was initially oriented to facilitate formation from the alkoxide/alkane-nearby state. Rotation of this structure and subsequent desorption (alkoxide/alkane reformation) completes the hydride transfer reaction. Desorption is analogous to the reverse reaction of the H-shared intermediate formation.

dx.doi.org/10.1021/cs1000619 |ACS Catal. 2011, 1, 105–115

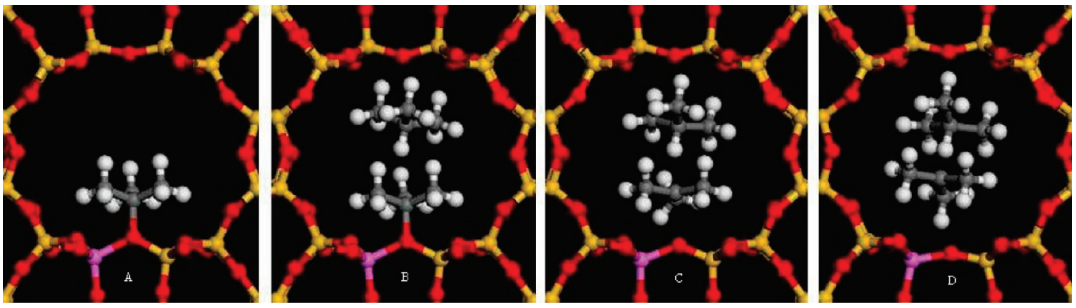

Figure 3. Intermediate and transition states along the reaction coordinate for hydride transfer from an alkane to an adsorbed alkoxide. A, *t*-butyl alkoxide; B, *t*-butyl alkoxide with isobutane nearby; C, transition state; D, shared hydride intermediate. Hydride transfer completes with rotation of the shared hydride intermediate and the inverse alkoxide/alkane reformation.

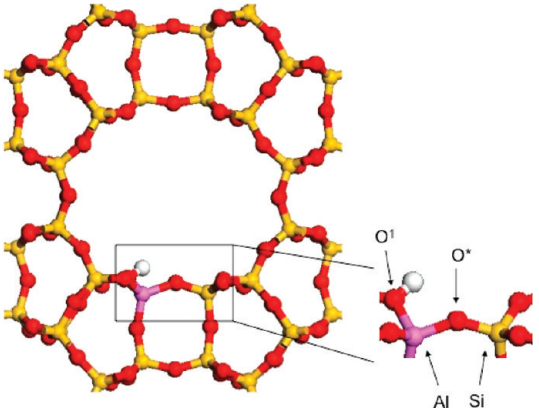

Figure 4. Mordenite active site with atom labels.

Alkoxide Formation Energy. Alkoxide formation may occur initially through alkene protonation. Alkoxide species are reformed during alkylation-hydride transfer cycles. To provide a consistent reference energy, formation energies were calculated by subtracting the sum of energies of the bare site ($E_{zeolite}$) and gas phase alkene (E_{alkene}) from the energy of the alkoxide ($E_{alkoxide}$):

$$\Delta E_{alkoxide\_formation} = E_{alkoxide} - (E_{zeolite} + E_{alkene}) \quad (1)$$

The formation energy for the methyl alkoxide was calculated by subtracting the sum of energies of the bare site and gas phase methane from the sum of energies of the alkoxide and gas phase hydrogen:

$$\Delta E_{alkoxide\_formation} = (E_{alkoxide} + E_{H_2}) - (E_{zeolite} + E_{methane}) \quad (2)$$

Alcohol Formation Energy. Gas phase alcohols serve as analogues for alkoxide species with C−O bonds. Trends in alcohol formation via alkene hydration are observed and compared with those of alkoxide formation. Alkene hydration energies were calculated by subtracting the sum of energies of gas phase water and a gas phase alkene species from the energy of the corresponding alcohol:

$$\Delta H_{alcohol\_formation} = H_{alcohol} - (H_{H_2O} + H_{alkene}) \quad (3)$$

For these calculations, formation enthalpies taken from the NIST Chemistry Webbook were used to provide the alcohol, water, and alkene energies.[39]

Alkane Entry Energy. Optimized structures with an alkane species near an alkoxide are the starting structures for hydride transfer reactions. The energy associated with moving the alkane from the gas phase into the alkoxylated zeolite pore, denoted the entry energy (ΔE_{entry}), was calculated by subtracting the sum of the energies of the alkoxylated zeolite ($E_{alkoxide}$) and the gas phase alkane (E_{alkane}) from the energy of the structure composed of the alkane incorporated into the pore nearby the alkoxide ($E_{alkane+alkoxide}$):

$$\Delta E_{entry} = E_{alkane+alkoxide} - (E_{alkoxide} + E_{alkane}) \quad (4)$$

Hydride Transfer Reaction Energy. Optimized H-shared species adsorbed within the zeolite pore were taken as intermediate states for the hydride transfer reaction. Previous studies[8−11,36] have suggested these structures may represent transition states or reaction intermediates. Though these were directly optimized as intermediates in this study, subsequent transition state searches were performed to determine if there was a higher energy state that preceded H-shared intermediate formation along the hydride transfer reaction path. Shared hydride complex formation energies were calculated by subtracting the energy of the alkoxide with an alkane nearby species ($E_{alkane+alkoxide}$) from the energy of the H-shared intermediate species ($E_{H\text{-}shared}$):

$$\Delta E_{H-shared\_formation} = E_{H-shared} - E_{alkane+alkoxide} \quad (5)$$

Hydride Transfer Activation Energy. Activation energies for hydride transfer were determined by subtracting the energy of the alkane nearby species from the energy of the transition state found along the path between that species and the H-shared intermediate:

$$E_{act} = E_{TS} - E_{alkane+alkoxide} \quad (6)$$

This E_{act} value represents the elementary reaction energy for the H-shared intermediate formation.

DFT-D. Optimizations with the DFT-D method as implemented in VASP[17,40] were performed for a subset of calculations. This package adds a semiempirical energy correction, accounting for long-range dispersion interaction effects, to the DFT energy computation:

$$E_{DFT+D} = E_{DFT} + E_{disp} \quad (7)$$

The dispersion term is calculated as the sum of atomic pair interactions over all atoms in the system, modeled by a function of the form:

$$E_{disp} = -s_6 \sum_{i=1}^{N_{at}-1} \sum_{j=i+1}^{N_{at}} \frac{\sqrt{C_6^i C_6^j}}{R_{ij}^6} f_{damp}(R_{ij}) \quad (8)$$

The s_6 term is a global scaling factor included to correct the differences that result from the choice of functional. This term, accepted to be 0.75 for the PBE functional,[17] was determined to

dx.doi.org/10.1021/cs1000619 |ACS Catal. 2011, 1, 105–115

Table 1. Dispersion Energies (in kJ mol^{-1}) Calculated with DFT-D for PW91 and PBE Functionals with s_6 = 0.75

	PW91	PBE
isobutane	−24	−24
t-butyl alkoxide	−1109	−1109
t-butyl alkoxide with isobutane nearby	−1230	−1232

be 0.75 for the PW91 functional as well by comparing dispersion energies calculated by both functionals. The dispersion energy, computed for the isolated isobutane molecule, adsorbed *t*-butyl alkoxide, and a structure with isobutane nearby a *t*-butyl alkoxide structure (Table 1) with each functional did not differ significantly (<0.03 eV).

The remaining terms in eq 8 are independent of the chosen functional. C_6 parameters are species dependent constants inherent to the atoms they represent, R_{ij} represent the interatomic distance between the two atoms, and f_{damp} is a damping function included to diminish the correction at short interatomic distances, which are accounted for in DFT calculations.

Structural optimizations were performed at the DFT-D level with starting structures taken from the DFT results. Dispersion corrections were added in a single-point calculation for transition states located by the NEB method.

RESULTS AND DISCUSSION

Alkoxide Formation. Methyl, ethyl (primary), propyl (secondary), and isobutyl (tertiary) alkoxides adsorbed to mordenite and ferrierite were optimized. Formation energies, calculated via eqs 1 and 2, are tabulated in Table 2.

Energies calculated with the DFT method indicate that the alkoxide formation process on both zeolites becomes less favorable and C−O^1 bond length increases as alkoxide substitution increases (Table 3). The alkoxide formation reaction via alkene protonation, forming a $R_3C-O_{zeolite}$ bond, is similar to an alcohol formation reaction from alkene hydration, forming a R_3C-OH bond, with the notable difference that the hydrocarbon products formed in the alkoxide formation processes are strained by the zeolite framework, whereas the products of alcohol formation reactions are not. Hydration energies calculated via eq 3 for the formation of alcohols with similar C−O bonds (i.e., *t*-butyl alkoxide and 1,1-dimethyl-ethanol have a similar C−O bond) become more exothermic as substitution of the oxygen bound carbon increases (Table 3), whereas the C−O bond distance remains approximately constant. The increase in endothermicity coupled with the increase in C−O^1 bond length observed as alkoxide substitution increases suggests steric repulsion occurs between the methyl substituents and zeolite framework. The calculated DFT adsorption energies for ferrierite are similar to those reported by Nieminen et al. using a QM/MM approach and the B3LYP functional.[41]

Campbell et al. showed that alkoxide formation also becomes slightly more favorable as alkoxide substitution increases for adsorption on a convex heteropolyacid surface.[42] The opposing trend observed for the concave mordenite pore also indicates steric repulsion occurs between the alkoxide and zeolite framework, as suggested by Benco et al. for alkoxide formation on gmelinite.[43] To ensure the trend did not result from repulsion between alkoxides residing in adjacent cells along the major pore axis, the formation energy of the *t*-butyl alkoxide was also calculated within a 1 × 1 × 2 supercell. The formation energy for a *t*-butyl alkoxide in this "double cell" is −20 kJ mol^{-1} for mordenite, which is effectively the same as the single cell formation energy (−19 kJ mol^{-1}). Similar C−O bond length trends were also observed for alkoxide formation on gmelinite.[43] Namuangruk et al. concluded that methyl repulsions between the ZSM-5 framework and the tertiary isobutene species lead to the less exothermic adsorption energy of isobutene among a series of butene isomers.[44]

The C−O bond distances observed for each alkoxide over ferrierite do not significantly differ from those observed over mordenite, indicating that the size of the zeolite pore does not affect the equilibrium distance achieved between the alkoxide and the zeolite framework. The less substituted alkoxides (methyl, ethyl, and propyl) are adsorbed stronger to ferrierite whereas the *t*-butyl alkoxide is more strongly bound to mordenite. Weaker adsorption of the *t*-butyl species to ferrierite likely arises from a pore size effect, as the smaller ferrierite pore leads to a greater degree of repulsive interactions between the *t*-butyl methyl groups and the pore. Stronger adsorption of the less substituted species on ferrierite may result from greater acid strength of ferrierite compared to mordenite. The periodic calculation approach does not allow for calculation of the deprotonation energy of the two zeolites because of the inability to represent the negatively charged conjugate base. Previous studies suggest the two deprotonation energies are similar (MOR[29] 1195 kJ mol^{-1}, FER[45] 1205 kJ mol^{-1}), though the values were calculated with different computational approaches.

When dispersion energy corrections are included, alkoxide formation energies are altered significantly, indicating dispersion energy contributions are significant in assessing hydride transfer energetics in zeolites. Previous studies have highlighted the inaccuracy of the pure DFT method in representing the alkoxide formation energy. For example, Tuma and Sauer[46−48] similarly reported that the tertiary alkoxide formation from isobutene on ferrierite is endothermic with a PW91, periodic DFT approach (17.2 kJ mol^{-1}),[46] but becomes exothermic (−66 kJ mol^{-1})[47] when a hybrid MP2:DFT periodic approach is employed. DFT+D formation energies are non-monotonic with substitution, and all adsorption energies are substantially more exothermic (Table 2). As the size of the alkoxide increases, the dispersion stabilization energy it experiences also increases, as given in Table 2. This stabilization competes with steric repulsions to give the non-monotonic behavior in alkoxide formation energy. Formation of the secondary alkoxide is therefore the most favorable. The DFT-D method causes slight geometry adjustments, as indicated by multiple steps taken in the DFT-D optimization when using DFT optimized structures as starting states. However, the C−O^1 bond distance does not change substantially upon structural optimization at the DFT-D level (Table 2).

Alkane Entry into the Alkoxylated Zeolite Pore. Intermediate structures with an alkane species optimized near an alkoxide structure (Figure 1b shows isobutane near the *t*-butyl alkoxide) were used as starting states for hydride transfer reactions. These constructions were optimized such that the transferred hydrogen atom was localized near the carbon atom of the alkoxide. Entry energies (eq 4) associated with moving the alkane from the gas phase to the pore-confined state are plotted versus degree of alkoxide substitution in Figure 5.

The entry energy is dependent on the size of the alkane species and alkoxide present within the pore. The DFT entry energy becomes increasingly endothermic as the two confined species become more substituted, with the methane-methyl value

Table 2. Alkoxide Formation Energies, C−O[1] Bond Distances, and Al−O*−Si Bond Angles

	$\Delta E_{alkoxide\ formation}$ (kJ mol^{-1})			C−O[1] bond distance (Å)			Al−O*−Si bond angle (°)	
	DFT	DFT-D	difference	DFT	DFT-D		DFT	DFT-D
				Mordenite				
						unit cell	142	143
t-butyl	−19	−92	−73	1.63	1.63	*t*-butyl	124	124
propyl	−50	−101	−51	1.56	1.56	propyl	129	129
ethyl	−64	−88	−24	1.52	1.52	ethyl	130	132
methyl	130[a]	114[a]	−16	1.48	1.49	methyl	132	133
				Ferrierite				
						unit cell	139	138
t-butyl	23	−87	−110	1.64	1.63	*t*-butyl	122	122
propyl	−59	−137	−77	1.56	1.55	propyl	128	128
ethyl	−79	−130	−51	1.51	1.51	ethyl	129	128
methyl	120[a]	96[a]	−24	1.49	1.49	methyl	132	132

[a] Formation energy for the methyl alkoxide was substantially higher than those calculated for the other alkoxides because this energy was determined for methane activation rather than alkene protonation. Therefore, it should not be used as a basis for comparison with the formation energies of the other species.

Table 3. Alcohol Formation Energies and C−O Bond Distances[a]

	$\Delta H_{alcohol\ formation}$ (kJ mol^{-1})	C−O bond distance (Å)
ethanol	−45	1.44
2-propanol	−51	1.45
1,1-dimethyl-ethanol	−53	1.45

[a] Alcohol formation energies were calculated with water, alcohol, and alkene formation energies from the NIST Chemistry Webbook.[39]

slightly exothermic (−9 kJ mol^{-1}) and the isobutane-*t*-butyl value highly endothermic (70 kJ mol^{-1}). The trend is due to repulsive interactions introduced between the confined species and the zeolite framework. Larger species take up more space within the pore, distorting the geometry of mordenite's framework. Oxygen atoms in the framework nearest the methyl groups of the alkane species are distorted, and this distortion provides further adjustments as tetrahedra restructure (see Figure 3). The alkyl species are compressed by the confined space of the pore, also altering their structures. For the *t*-butyl-isobutane species, the alkoxide C−O bond is shortened by 0.03 Å, and the C−C bonds of isobutane are compressed by 0.01 Å relative to their gas phase values. Geometric distortions in both the confined species and the framework become less evident as the size of the confined species decreases.

Dispersion interactions drastically alter trends in entry energy with respect to degree of substitution. All entry energies become significantly more exothermic. Entry into the mordenite pore, for all alkane/alkoxide combinations, is exothermic with DFT-D. For methyl and ethyl alkoxides, the alkane entry energy becomes more exothermic with increasing alkane substitution, because of the greater dispersion stabilization of the larger species. Increasing dispersion stabilization with increasing chain length is clearly expected, though the increase in adsorption energy between methane and ethane exceeds the 8.5 kJ mol^{-1} per additional carbon reported by De Moor et al.[49] using an embedded QM/MM model and the MP2 method. A possible source of the

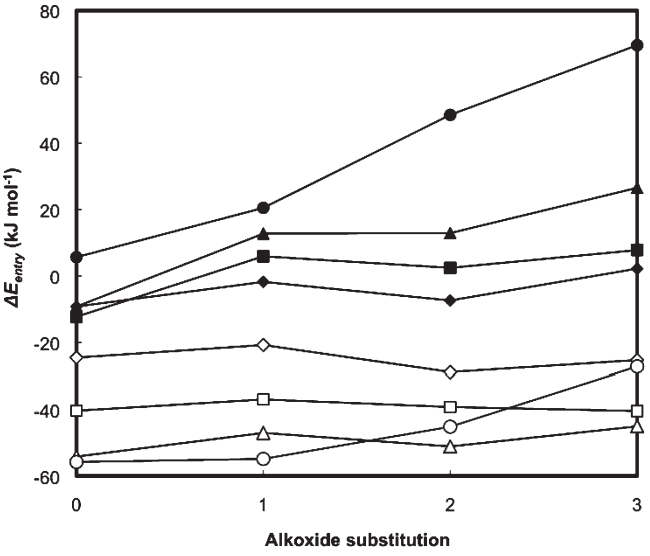

Figure 5. DFT (filled) and DFT-D (opened) entry energy versus alkoxide substitution−mordenite. Entering species: methane, ♦; ethane, ■; propane, ▲; isobutane, ●.

difference is a stronger dispersive interaction facilitated by the alkoxide species as opposed to solely the faujasite pore considered by De Moor et al.[49] For larger alkoxides, competition between dispersion stabilization and electrostatic repulsion interactions is seen as the confined species fill the pore's capacity. For example, entry of ethane into mordenite with an isobutyl alkoxide is favored over isobutane entry, indicating that for larger confined species, repulsions begin to significantly destabilize this hydride transfer precursor state. Despite the energetic changes observed upon incorporation of dispersion corrections, the geometries did not change significantly for any of the optimized structures.

The DFT-D entry of isobutane over a *t*-butyl alkoxide in ferrierite was calculated to be 126 kJ mol^{-1}, (282.9 kJ mol^{-1} when calculated at DFT level) significantly higher than that of isobutane over a *t*-butyl alkoxide in mordenite. An increase in this

dx.doi.org/10.1021/cs1000619 |ACS Catal. 2011, 1, 105–115

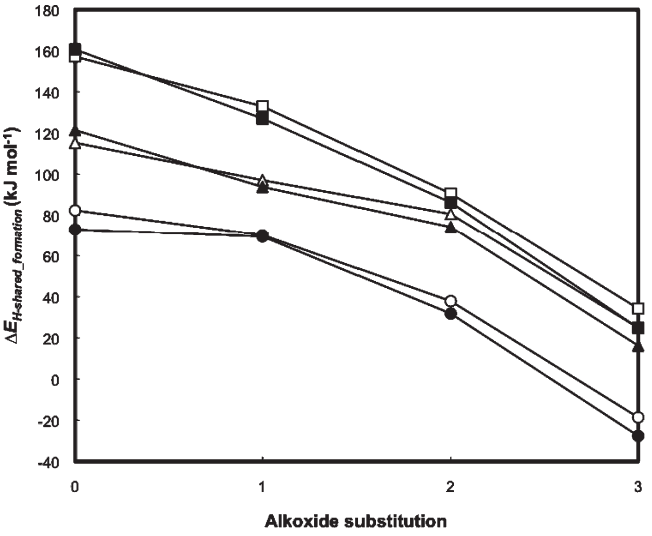

Figure 6. DFT (filled) and DFT-D (opened) shared hydride intermediate formation energies − mordenite. H-donating species: ethane, ■; propane, ▲; isobutane, ●.

energy was expected given the smaller size of the ferrierite pore. This energy is highly endothermic, indicating dispersion interactions are not significant enough to overcome the strong repulsive interactions induced upon the structure by the ferrierite's pore framework. The pore is much more constricted in ferrierite than in mordenite, leading to higher repulsive interactions between the confined species and zeolite framework, which greatly increase the energy required to introduce the alkane into the pore. Again, the geometry of both the zeolite framework and the confined species is distorted. The length of the alkoxide C−O bond is reduced by 0.07 Å. The C−C bond of isobutane nearest the pore wall decreases by 0.02 Å relative to the C−C bond of a gas phase isobutane molecule. The other C−C bonds are decreased by 0.02 Å relative to gas phase.

Shared Hydride Intermediate Formation. Shared hydride complexes (Figure 3d) were optimized for various combinations of hydrogen donor and acceptor substitution. In these structures, a net positive charge is shared between two alkyl fragments, one initiating from the alkoxide, the other from the alkane. A C−H−C three centered, two electron bond is formed. Shared hydride complexes generated from a methane donor are unstable and could not be optimized. Shared hydride complexes generated by a methyl alkoxide or an ethane donor and a propyl or ethyl alkoxide represent transition states, and are discussed further in the following section. Optimization attempts with a methane donor species led either to regeneration of the methane molecule and the alkoxide species or deprotonation of the alkoxide fragment, generating an alkene and methane. Methane is unable to donate a significant portion of electron density to stabilize the positive charge on the carbonium fragment. Reaction energies for converting the alkane nearby structure to a shared hydride intermediate, calculated via eq 5, are depicted in Figure 6.

For DFT and DFT-D results, generation of the shared hydride intermediate becomes more favorable as the substitution of the alkoxide, the hydride acceptor, increases. The relative strength of the C−O alkoxide bond broken in the formation of the shared hydride complex contributes to this observed trend. Less substituted alkoxides are more strongly bound to the zeolite surface. To form the shared hydride intermediate, the covalent C−O bond between the alkoxide and zeolite framework has to be broken. Additionally, more highly substituted alkoxide fragments can better stabilize the net positive charge that is localized upon them in the shared hydride intermediate structure.

Table 4. Alkane Fragment C−H Bond Displacement (in Å) upon Shared Hydride Intermediate Formation (DFT-D Results)[a]

alkoxide	ethane	propane	isobutane
t-butyl	0.01	0.06	0.12
propyl	0.05	0.12	0.19
ethyl	0.13	0.18	0.29
methyl	0.16	0.29	0.77

[a] C−H bond distances are given in the Supporting Information, Table S1.

Generation of the shared hydride intermediate also becomes more favorable as the substitution of the donating alkane species increases. During the formation process, the C−H bond associated with the hydrogen donor molecule extends (Table 4, Supporting Information, Table S1). Less-substituted alkyl fragments require a greater extent of stabilization when localized with a net positive charge. To attain this stabilization, the alkoxide fragments with low substitution transfer larger portions of the positive charge to the alkane fragment, manifested in the displacement of the shared hydrogen atom from the alkane donor. Atomic charges calculated with the Bader approach were also evaluated, and are consistent with the conclusion based on bond displacements. Net charges on the individual alkyl fragments in the shared hydride state are given in Supporting Information, Table S2. Highly substituted alkanes are able to readily stabilize positive charges localized upon them, accepting a larger portion of the net positive charge in the shared hydride intermediate and allowing the shared hydrogen atom to extend farther away than do less substituted species.

For isobutane interacting with a *t*-butyl alkoxide, formation of the shared hydride intermediate is an exothermic process. The shared hydride intermediate is able to localize within the center of the mordenite pore, minimizing repulsive interactions with the zeolite framework. The strain introduced in the zeolite lattice at the alkoxide site in the alkane nearby state is relaxed in the shared hydride structure (see Figure 3). The intermediate is also readily able to stabilize the net positive charge it experiences, sharing it between two tertiary alkyl fragments.

Dispersion corrected shared hydride formation energies are slightly more endothermic for most combinations of species than shared hydride formation energies determined from DFT results. Exceptions are observed for formation of shared hydride intermediates with a methyl alkoxide fragment and propane or ethane alkane fragment. Dispersion interactions stabilize both the initial alkane species within the alkoxylated zeolite and the product shared hydride intermediates. The starting species contain alkoxide structures localized very near the zeolite framework. Resultantly, these structures are more stabilized by dispersion interactions than shared hydride intermediates, which minimize repulsive interactions with the zeolite framework by migrating to the center of the pore. The geometries of optimized shared hydride species are not significantly altered by inclusion of dispersion energy corrections.

Transition States for Shared Hydride Formation. Transition states were determined by examining the minimum energy path between the alkane nearby alkoxide (Figure 3b) and shared hydride intermediate (Figure 3d) structures. For most cases, the

dx.doi.org/10.1021/cs1000619 |*ACS Catal.* 2011, 1, 105–115

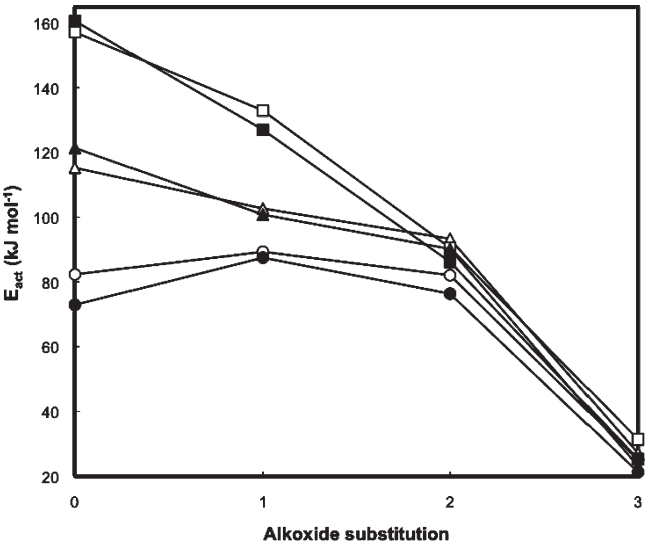

Figure 7. DFT (filled) and DFT-D (opened) activation energies for elementary step of shared hydride complex formation—mordenite. H-donating species: ethane, ■; propane, ▲; isobutane, ●.

Table 5. Alkane Fragment C—H Bond Displacement (Å) Relative to Alkane Nearby Structure for Transition State Structures[a]

alkoxide	ethane	propane	isobutane
t-butyl	0.00	−0.01	0.01
propyl	0.05[b]	0.02	0.05
ethyl	0.13[b]	0.07	0.08
methyl	0.16[b]	0.29[b]	0.77[b]

[a] C—H bond distances are given in the Supporting Information, Table S1 [b] For all methyl, propyl-ethane, and ethyl-ethane species, the shared hydride intermediate was found to be the transition state rather than a carbenium ion.

transition state is a carbenium ion generated upon departure of the alkoxide from the zeolite surface (Figure 3c). Exceptions are seen for transition states for hydride transfer to methyl alkoxides and for transfer from ethane to a propyl or ethyl alkoxide. For these structures, the shared hydride structure is determined to be a transition state, with no higher energy state preceding it along the reaction coordinate. Activation energies, calculated via eq 6, are depicted in Figure 7. These values represent the energy barrier associated with forming a shared hydride intermediate from an alkoxide and alkane species localized within the alkoxylated pore, an elementary step in the hydride transfer reaction path.

Activation energy decreases as alkoxide substitution increases for all cases for calculation at both DFT and DFT-D levels. Carbenium ions generated in the formation process are electron deficient. More highly substituted carbenium ions experience better positive charge stabilization, and, consequently, have lower activation energies. Activation energy also decreases as hydrogen donor substitution increases; however, this trend diminishes as the substitiution of the alkoxide fragment increases. Transition state C—H bond distance variations, associated with the shared hydrogen C—H bond of the alkane fragment, are tabulated in Table 5. Observed trends are similar to those for shared hydride intermediate stabilization, and Bader charges (Supporting Information, Table S3) on the alkyl fragments provide further agreement with the analysis based on bond displacements.

Partial transfer of the electron density from the alkane fragment to the alkoxide fragment occurs at the transition state as evidenced by extension of the alkane C—H bond. As the carbenium ion's substitution decreases, it becomes less stable, requiring a larger donation of electron density from the alkane fragment and causing the C—H bond associated with the donor to displace. Transition states initiating from *t*-butyl alkoxides are the most stable and do not displace the alkane C—H bond significantly, causing the activation energy associated with the formation of such transition states to be nearly independent of the substitution of the alkane hydride donor.

DFT-D energies were determined by running single point calculations on transition state structures found with the DFT method. DFT and DFT-D energies are similar in magnitude and display the same trends. At lower alkoxide fragment substitution, activation energy decreases as the substitution of the H-donor increases. Agreement between activation energies determined with and without disperison corrections indicates that generation of the shared hydride complex is governed by bond breaking-forming processes and not dispersion interactions with the zeolite framework.

Overall Hydride Transfer Reaction Path. The overall hydride transfer reaction path is presented in Figure 8 for transfer between isobutane and a *t*-butyl alkoxide using DFT-D energies. The reaction is considered to initiate from the *t*-butyl alkoxide and gas phase isobutane. Alkoxide formation, an exothermic process for the *t*-butyl species, with a DFT-D formation energy of −92 kJ mol^{-1} relative to the mordenite unit cell and gas phase isobutene, is not included in Figure 8. Incorporating the H-donor (isobutane) into the alkoxylated zeolite pore is an exothermic process, releasing 27 kJ mol^{-1}. Once in the pore, formation of the shared hydride intermediate from the confined isobutane species and the *t*-butyl alkoxide has a barrier of 25 kJ mol^{-1}. The shared hydride species generated in this process is energetically favored over the *t*-butyl alkoxide, indicating that this shared hydride complex exists as a stable species rather than a metastable, reactive intermediate, an observation that is contrary to that determined by Boronat et al. for zeolite catalyzed hydride transfer between two tertiary fragments.[10] Boronat modeled the active site only, as a cluster consisting of one aluminum and two silicon tetrahedra whereas we used a periodic model. The stability of the positively charged shared hydride species relative to the alkoxide is consistent with later work by the same authors, which used the ONIOM approach to model the entire mordenite pore and located a tertiary carbenium ion that is stable relative to the alkoxide.[50]

The hydride transfer reaction is completed by rotating the shared hydride species within the pore and reversing the shared hydride formation steps to generate an alkoxide from the H-donor. Rotation of the shared-hydride species by 90 degrees increases the energy by 10 kJ mol^{-1}, indicating that rotation is facile. In the case of isobutane interacting with a *t*-butyl alkoxide, the overall reaction is symmetric, and the generation of the *t*-butyl alkoxide from the shared hydride complex is represented by the reverse of the shared hydride formation process. The limiting barrier for the overall isobutane to *t*-butyl alkoxide transfer is 44 kJ mol^{-1}, which is the barrier for the elementary reaction of converting the shared hydride species back to an alkoxide plus alkane.

The overall hydride transfer reaction path is also presented for transfer between ethane and a propyl alkoxide in Figure 9. Incorporation of the ethane H-donor into the alkoxylated zeolite pore is an exothermic process, lowering the system's energy by 40 kJ mol^{-1}. A barrier of 91 kJ mol^{-1} is associated with formation

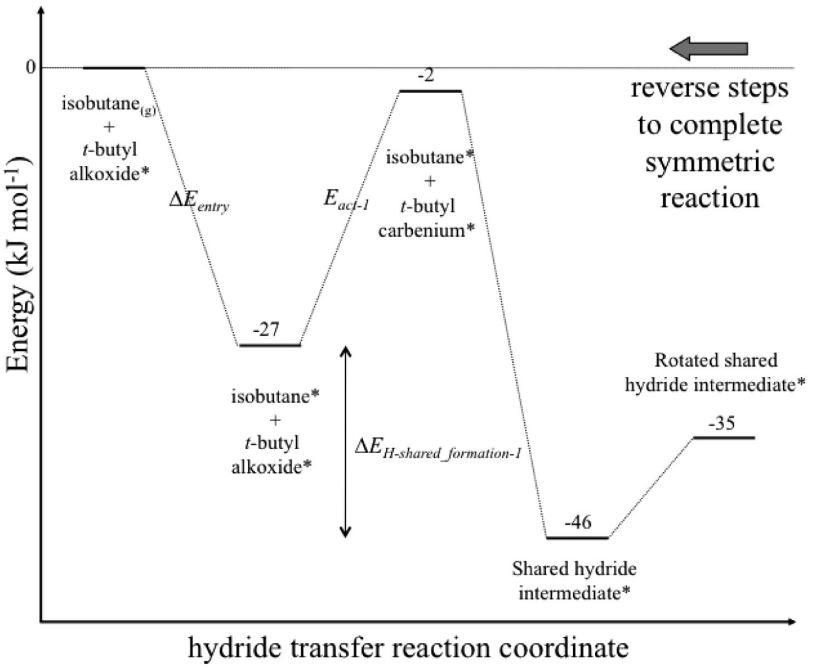

Figure 8. Reaction path for hydride transfer between isobutane and a *t*-butyl alkoxide−mordenite referenced from the *t*-butyl alkoxide and isobutane in the gas phase (DFT-D energies).

of the shared hydride complex from this confined species. The shared hydride complex generated in this process is unstable, representing a transition state rather than a reactive intermediate. To complete the hydride transfer reaction, the shared-hydride species must rotate 180° to position the ethyl fragment closer to the conjugate anion site. The energetics associated with intermediate degrees of rotation of this species within the pore were not considered. The shared hydride structure generated after 180° rotation is 6 kJ mol^{-1} higher in energy than that with the propyl fragment localized near the active site, resulting from a partial shift of positive charge localization from the propyl fragment to the ethyl fragment. An activation barrier of 6 kJ mol^{-1} exists for the generation of propane and the ethyl alkoxide from the shared hydride intermediate. The hydride transfer reaction is completed by removal of propane from the pore, an endothermic process requiring 47 kJ mol^{-1} to proceed.

The overall barrier to hydride transfer between propane and the ethyl alkoxide is 115 kJ mol^{-1}, as determined by Murdoch's procedure.[51] This barrier represents the energy difference between the structure consisting of propane interacting with the ethyl carbenium ion and the structure with ethane localized in the pore near the propyl alkoxide. Hydride transfer from propane to the ethyl alkoxide is represented by the reverse of the reaction coordinate depicted in Figure 9. The overall barrier to this transfer is 103 kJ mol^{-1}, given by the barrier to form the shared-hydride intermediate from the ethyl alkoxide and propane. Both propane to ethyl alkoxide and ethane to propyl alkoxide hydride transfer share the same highest energy transition state, with their apparent barriers differing because of the different stable intermediate states.

The overall barrier to hydride transfer, as determined by Murdoch's procedure[51] with DFT and DFT-D methods, is presented for all combinations of alkoxide and H-donor substitution in Table 6. This barrier is higher for DFT results, in most cases, because of the high energies associated with bringing the

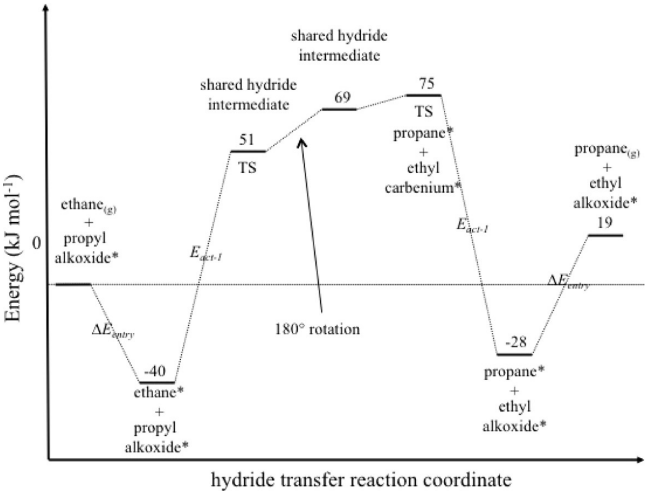

Figure 9. Reaction path for hydride transfer between ethane and the propyl alkoxide−mordenite referenced from the propyl alkoxide and ethane in the gas phase (DFT-D energies).

H-donor into the zeolite pore. Entry energy decreases as the substitution of the alkoxide or H-donor decreases, resulting in less differentiation between overall barriers calculated from DFT and DFT-D results. For DFT-D results, H-donor entry becomes an exothermic process, and the overall barrier to hydride transfer involves formation of a shared hydride complex from the alkoxide species and pore confined H-donor for all cases except that of hydride transfer between isobutane and the *t*-butyl alkoxide. Considering the DFT-D values, there is a substantial increase in the barrier for hydride transfer if either the acceptor or the donor does not contain a tertiary carbon atom. However, we note that the DFT-D entry energy to add isobutane into the ferrierite pore near to an isobutyl alkoxide is 126 kJ mol^{-1},

dx.doi.org/10.1021/cs1000619 |*ACS Catal.* 2011, 1, 105–115

Table 6. Summary of Overall Energy Barriers to Hydride Transfer

hydride transfer			overall barrier (kJ mol^{-1})	
to	from	product	DFT	DFT-D
t-butyl alkoxide	isobutane	*t*-butyl alkoxide + isobutane	91	44
	propane	propyl alkoxide + isobutane	105	82
	ethane	ethyl alkoxide + isobutane	90	95
propyl alkoxide	isobutane	*t*-butyl alkoxide + propane	125	82
	propane	propyl alkoxide + propane	103	93
	ethane	ethyl alkoxide + propane	116	114
ethyl alkoxide	isobutane	*t*-butyl alkoxide + ethane	108	89
	propane	propyl alkoxide + ethane	114	103
	ethane	ethyl alkoxide + ethane	133	133

indicating that smaller pores may prefer hydride transfer among less substituted species because of the difficulty of accommodating both species. Pore structure will also likely impact entropic differences along the hydride transfer reaction path. The located transition states and shared hydride intermediates have no direct covalent bonding with the zeolite, and rotation of the shared-hydride intermediate may impact the hydride transfer rate. The balance between the enthalpic and the entropic effects involved in the hydride transfer reaction could be investigated using an ab initio molecular dynamics approach similar to that recently applied by Bucko et al.[52]

CONCLUSIONS

Density functional theory calculations suggest that zeolite-catalyzed hydride transfer between alkane species and chemisorbed alkoxides proceeds through the formation of shared hydride carbonium ion complexes. These complexes represent reactive intermediates or transition states unless hydride transfer occurs between tertiary carbons of the donor and acceptor species. For hydride transfer between isobutane and the *t*-butyl alkoxide, the shared hydride structure represents a stable species. This result is contrary to that determined by zeolite cluster models, suggesting that the extended pore structure is necessary to properly consider the hydride transfer reaction. In most cases, the hydride transfer reaction proceeds through the formation of carbenium ion transition states, with exceptions arising for hydride transfer between species of low carbon substitution in which cases shared hydride structures represent transition states.

The inclusion of dispersion interactions is necessary to represent the energy change associated with an alkane entering the zeolite pore. Inclusion of dispersion corrections, however, does not significantly influence the geometries or stability of intermediate structures along the hydride transfer reaction path or the activation barriers associated with the elementary step of formation of the shared hydride complex. These findings suggest that dispersion interactions are insignificant in directing the energetics of C_1-C_4 reactive species which are localized within the mordenite pore. Because entry of the alkane into the mordenite pore can be endothermic as calculated without dispersion interactions, the overall hydride transfer barrier may be misrepresented by DFT when referenced to the separate alkane species. These results suggest that dispersion interactions must be considered to properly examine hydride transfer occurring in zeolite catalysts.

The overall barrier to hydride transfer over mordenite, as determined by Murdoch's procedure[51] with dispersion corrected energies, decreases as the substitution of the hydride donor or acceptor species increases. These barriers are associated with the formation of a shared hydride species from the alkoxide and an alkane/hydride donor species localized within the zeolite pore for all combinations of hydride donor and acceptor substitution except for two tertiary species. For hydride transfer between two tertiary species, the overall barrier to hydride transfer is associated with regeneration of the alkoxide from the stable shared hydride intermediate and removal of the alkane species from the mordenite pore.

ASSOCIATED CONTENT

Supporting Information. C−H bond distances associated with carbon atoms involved in hydride transfer, for all equilibrium and transition states, and partial charges on the alkyl fragments within the shared hydride states. This material is available free of charge via the Internet at http://pubs.acs.org.

AUTHOR INFORMATION

Corresponding Author
*E-mail: mjanik@psu.edu. Phone: (814)863-9366.

ACKNOWLEDGMENT

The Penn State Materials Simulation Center (MSC) and Research Computing and Cyberinfrastructure group (RCC) are acknowledged for their technical support.

REFERENCES

(1) Corma, A. *Chem. Rev.* **1995**, *95*, 559–614.
(2) Feller, A.; Zuazo, I.; Guzman, A.; Barth, J. O.; Lercher, J. A. *J. Catal.* **2003**, *216*, 313–323.
(3) Weitkamp, J.; Traa, Y. *Catal. Today* **1999**, *49*, 193–199.
(4) Simpson, M. F.; Wei, J.; Sundaresan, S. *Ind. Eng. Chem. Res.* **1996**, *35*, 3861–3873.
(5) Cardona, F.; Gnep, N. S.; Guisnet, M.; Szabo, G.; Nascimento, P. *Appl. Catal., A* **1995**, *128*, 243–257.
(6) Platon, A.; Thomson, W. J. *Appl. Catal., A* **2005**, *282*, 93–100.
(7) Frash, M. V.; Solkan, V. N.; Kazansky, V. B. *J. Chem. Soc., Faraday Trans.* **1997**, *93*, 515–520.
(8) Kazansky, V. B.; Frash, M. V.; van Santen, R. A. *Catal. Lett.* **1997**, *48*, 61–67.
(9) Boronat, M.; Zicovich-Wilson, C. M.; Corma, A.; Viruela, P. *Phys. Chem. Chem. Phys.* **1999**, *1*, 537–543.
(10) Boronat, M.; Viruela, P.; Corma, A. *J Phys. Chem. A* **1998**, *102*, 9863–9868.

(11) Janik, M. J.; Davis, R. J.; Neurock, M. *J. Catal.* **2006**, *244*, 65–77.
(12) Yoo, K.; Burckle, E. C.; Smirniotis, P. G. *J. Catal.* **2002**, *211*, 6–18.
(13) Corma, A.; Martinez, A.; Martinez, C. *Catal. Lett.* **1994**, *28*, 187–201.
(14) Wesolowski, T. A.; Parisel, O.; Ellinger, Y.; Weber, J. *J. Phys. Chem.* **1997**, *101*, 7818–7825.
(15) Zhang, Y.; Pan, W.; Yang, W. *J. Chem. Phys. A* **1997**, *107*, 7921–7925.
(16) Grimme, S. *J. Comput. Chem.* **2004**, *25*, 1463–1473.
(17) Grimme, S. *J. Comput. Chem.* **2006**, *27*, 1787–1799.
(18) Kresse, G.; Hafner, J. *Phys. Rev. B: Solid State* **1993**, *47*, 558–561.
(19) Kresse, G.; Furthmüller, J. *Phys. Rev. B: Solid State* **1996**, *54*, 11169–11186.
(20) Kresse, G.; Furthmüller, J. *Comput. Mater. Sci.* **1996**, *6*, 15–50.
(21) Vanderbilt, D. *Phys. Rev. B: Solid State* **1990**, *41*, 7892–7895.
(22) Perdew, J. P.; Chevary, J. A.; Vosko, S. H.; Jackson, K. A.; Pederson, M. R.; Singh, D. J.; Fiolhais, C. *Phys. Rev. B: Solid State* **1992**, *46*, 6671–6687.
(23) Mills, G.; Jónsson, H.; Schenter, G. K. *Surf. Sci.* **1995**, *324*, 305–337.
(24) Henkelman, G.; Jonsson, H. *J. Chem. Phys.* **2000**, *113*, 9978–9985.
(25) Henkelman, G.; Uberuaga, B. P.; Jonsson, H. *J. Chem. Phys.* **2000**, *113*, 9901–9904.
(26) Mortier, W. J.; Pluth, J. J.; Smith, J. V. *Mater. Res. Bull.* **1976**, *11*, 15–21.
(27) Schlenker, J. L.; Pluth, J. J.; Smith, J. V. *Mater. Res. Bull.* **1979**, *14*, 751–758.
(28) Schlenker, J. L.; Pluth, J. J.; Smith, J. V. *Mater. Res. Bull.* **1979**, *14*, 849–856.
(29) Brandle, M.; Sauer, J. *J. Am. Chem. Soc.* **1998**, *120*, 1556–1570.
(30) Alberti, A. *Zeolites* **1997**, *19*, 411–415.
(31) Monkhorst, H. J.; Pack, J. D. *Phys. Rev. B: Solid State* **1976**, *13*, 5188.
(32) Vaughan, P. *Acta Crystallogr.* **1966**, *21*, 983–990.
(33) Tuma, C.; Sauer, J. *Phys. Chem. Chem. Phys.* **2006**, *8*, 3955–3965.
(34) Kazansky, V. B.; Senchenya, I. N. *J. Catal.* **1989**, *119*, 108–120.
(35) van Santen, R. A. *Catal. Today* **1997**, *38*, 377–390.
(36) Kazansky, V. B. *Catal. Today* **1999**, *51*, 419–434.
(37) Bhan, A.; Joshi, Y. V.; Delgass, W. N.; Thomson, K. T. *J. Phys. Chem. B* **2003**, *107*, 10476–10487.
(38) Choudhary, V. R.; Kinage, A. K.; Choudhary, T. V. *Science* **1997**, *275*, 1286–1288.
(39) Afeefy, H. Y.; Liebman, J. F.; Stein, S. E. . In *NIST Chemistry WebBook*; Linstrom, P. J.; Mallard, W. G., Eds.; NIST Standard Reference Database Number 69; National Institute of Standards and Technology: Gaithersburg, MD.
(40) Svelle, S.; Tuma, C.; Rozanska, X.; Kerber, T.; Sauer, J. *J. Am. Chem. Soc.* **2008**, *131*, 816–825.
(41) Nieminen, V.; Sierka, M.; Murzin, D. Y.; Sauer, J. *J. Catal.* **2005**, *231*, 393–404.
(42) Campbell, K. A.; Janik, M. J.; Davis, R. J.; Neurock, M. *Langmuir* **2005**, *21*, 4738–4745.
(43) Benco, L.; Hafner, J.; Hutschka, F.; Toulhoat, H. *J. Phy. Chem. B* **2003**, *107*, 9756–9762.
(44) Namuangruk, S.; Tantanak, D.; Limtrakul, J. *J. Mol. Catal. A: Chem.* **2006**, *256*, 113–121.
(45) Haase, F.; Sauer, J. *Microporous Mesoporous Mater.* **2000**, *35−36*, 379–385.
(46) Tuma, C.; Sauer, J. *Angew. Chem.* **2005**, *117*, 4847–4849.
(47) Tuma, C.; Sauer, J. *Phys. Chem. Chem. Phys.* **2006**, *8*, 3955–3965.
(48) Tuma, C.; Sauer, J. *Angew. Chem.* **2010**, *49*, 4678–4680.
(49) De Moor, B. A.; Reyniers, M.-F.; Marin, G. B. *Phys. Chem. Chem. Phys.* **2009**, *11*, 2939–2958.
(50) Boronat, M.; Viruela, P. M.; Corma, A. *J. Am. Chem. Soc.* **2004**, *126*, 3300–3309.
(51) Murdoch, J. R. *J. Chem. Educ.* **1981**, *58*, 32–36.
(52) Bucko, T.; Benco, L.; Hafner, J.; Angyan, J. G. *J. Catal.* **2007**, *250*, 171–183.